https://doi.org/10.5194/wes-2026-143
Preprint. Discussion started: 25 August 2026

Open Access
WIND ENERGY SCIENCE
DISCUSSIONS

WIX: a wakeness index for preliminary assessment of regional wind farm wake interactions

Nicolas G. Alonso-de-Linaje[1], Andrea N. Hahmann[1], and Alfredo Peña[1]

[1]DTU Wind and Energy Systems, Frederiksborgvej 399, 4000 Roskilde, Denmark

Correspondence: Nicolas G. Alonso-de-Linaje (nicdel@dtu.dk)

Abstract. The rapid clustering of large offshore wind farms in the North Sea and other coastal areas in the world raises concerns about compounded wake losses that propagate for tens of kilometres. Simulating these regional wakes with wind farm parameterisations in numerical weather prediction models is however computationally prohibitive for multi-scenario planning, as each change in layout or turbine specification demands a new simulation. We showcase the Wakeness Index (WIX), a geometry-based indicator that produces rapid, first-order estimates of climatological wake footprints from only three inputs: turbine coordinates and rotor diameters, wind direction frequency statistics, and a single tuneable decay factor df. The WIX is here calibrated against year-long simulations using the Weather Research and Forecasting (WRF) model with the Fitch wind farm parameterisation for current, and projected 2030 and 2050 North Sea scenarios, using the footprints' intersection-over-union (IoU) at the 92, 95, and 98% wind speed recovery levels and the pixel-wise coefficient of determination R^2 for the velocity deficit field. The footprint optimum over all scenarios ($df = 2.3$, mean IoU $= 0.75$) is adopted as the operating point. The future, higher-density layouts are reproduced skilfully and share common optima (IoU up to 0.87, R^2 up to 0.92), demonstrating generalisability across comparable turbine populations. The WIX transfers to the more stable regime of the Baltic Sea without region-specific tuning, and wind direction frequencies from the New European Wind Atlas (NEWA) dataset can substitute the WRF-derived wind direction frequency statistics with near-perfect agreement, removing the dependency on output from localized simulations. Computing the WIX over the entire North Sea is reduced to a few seconds on 32 CPUs, against the CPU-weeks required by the WRF model, the WIX is well suited as a lightweight pre-feasibility screening tool for early-stage wind farm and marine spatial planning.

1 Introduction

Despite its deceleration in the mid 2020s, offshore wind energy development in the North Sea has reached an unprecedented pace over the previous decade, driven by ambitious decarbonization targets and favorable wind resources (Elizalde et al., 2026; WindEurope, 2024). Ever-larger wind farms are now being planned in close proximity, and some countries, e.g., Denmark, Germany, the Netherlands, and the United Kingdom, envision interconnected energy islands that will further intensify inter-farm interactions. Such clustering raises concerns about compounded wake losses that can propagate for tens of kilometres, adversely affecting the overall efficiency of the regional wind energy system (Volker et al., 2015; Borgers et al., 2024).

https://doi.org/10.5194/wes-2026-143
Preprint. Discussion started: 25 August 2026

eawe european academy of wind energy
Open Access WIND ENERGY SCIENCE DISCUSSIONS

Regional wake analyses are typically conducted with wind farm parameterisations (WFPs) embedded in numerical weather prediction (NWP) models such as the Weather Research and Forecasting (WRF) model (Skamarock et al., 2019). Widely used WFPs include the explicit wind farm parameterisation (EWP) (Volker et al., 2015; García-Santiago et al., 2026), the MAV scheme (Ma et al., 2022), and the Fitch scheme (Fitch et al., 2012). Although NWP models' WFPs resolve the mesoscale physics required to simulate long-range wakes, they come with a substantial computational burden: a single wind farm scenario in a one-year WRF model simulation with thousands of offshore turbines can demand hundreds of core hours and terabytes of storage. As a result, exploring numerous wind farm layouts, capacity densities, and rotor diameters becomes prohibitively expensive, restricting the ability of stakeholders to perform an optimised spatial planning of wind energy and other marine activities. In this particular case, the computational burden of NWPs is a bottleneck by design, since we have to redo the simulation every time the wind farm layout or wind turbine characteristics are changed. This is a practical rather than a hypothetical constraint: national deployment plans (Hahmann et al., 2025) are revised on a timescale of months as tender outcomes, capacity targets, and area designations evolve, so a layout that motivated a year-long simulation may be superseded before the results are analysed. Each revision resets the modelling effort, which is precisely the situation a fast screening tool is meant to relieve.

Alternative methods for assessing regional wakes include analytical models (Frandsen, 1992; Calaf et al., 2010), high fidelity simulations (van der Laan et al., 2023), and engineering wake models (Bastankhah and Porté-Agel, 2014; Warder and Piggott, 2025). However, none of these models typically account for atmospheric dynamics above and in between wind farm clusters, which are essential for accurately modelling wind farm wakes on a regional scale and determining their footprint (Allaerts and Meyers, 2019; Lundquist et al., 2018).

We refer to the wake footprint as the area influenced by the wake of a wind farm cluster at a given instant, and to the climatological wake footprint as the area influenced by the long-term mean wake of that cluster. For modeling climatological wake footprints, NWP models remain one of the primary resources for a variety of stakeholders, including national authorities and private developers, due to the lack of alternative tools that can reliably provide wake footprints and annual energy production estimates for entire regions. To lower the entry barrier for regional wake assessments, we showcase the Wakeness Index (WIX) for preliminary multi-scenario screening. Initially introduced in Alonso-De-Linaje et al. (2025), the WIX is a geometry-based indicator that combines three readily available inputs: (i) turbine coordinates and rotor diameters, (ii) site-specific wind direction frequency statistics, and (iii) a single tuneable parameter accounting for the wake decay with distance from the turbine. Once the WIX is configured, planners can modify farm shapes, spacings, or turbine specifications and instantly obtain a first-order estimate of wake impacts without rerunning a full NWP model.

The WIX is designed to approximate the climatological wake footprints produced by a NWP model, while relying on the skill of NWP models in simulating such wakes. We assume that the reference numerical simulations are trusted by users; consequently, the WIX is intended to be tunable using any numerical simulation framework that a potential user may wish to evaluate or extend. In this sense, the WIX provides guidance on the expected wake effects over a region of interest, when assessing its potential for wind energy harvesting. Higher WIX values indicate a greater chance of wakes impacting the investigated area. Due to its computational efficiency, the WIX can be mapped across several hypothetical wind farm layouts within

https://doi.org/10.5194/wes-2026-143
Preprint. Discussion started: 25 August 2026

seconds, providing an effective preliminary assessment before investing resources in NWP runs, high-fidelity simulations, or field campaigns. From a marine planning perspective, the resulting wake footprints can be superimposed on maps of shipping lanes, protected areas, or fisheries activities, allowing for the quick identification of conflicts and synergies.

This work is organised as follows. Section 2 describes the wind farm datasets for the current, Y2030, and Y2050 wind farm deployment scenarios, as well as the WRF model simulations used to generate the reference wind speed deficit fields. Section 3 introduces the WIX and the optimisation procedure for the decay factor. Section 4 presents the decay factor calibration and verification results against a different scenario, including the spatial assessment of the Y2030 and Y2050 scenarios, the regional wake footprint analysis at different wind speed recovery thresholds, the substitution of our simulation-derived wind direction frequencies with publicly available data, the evaluation of the WIX under the distinct atmospheric regimes of the Baltic Sea, and the application to three hypothetical wind farm clusters as a pre-feasibility demonstration of the WIX. Section 5 discusses the scope and limitations of the WIX and Section 6 summarises the main findings and method.

2 Data

2.1 Wind farm datasets for the current, 2030, and 2050 future scenarios

We use wind farm layouts for the November 2021 (CURRENT) and for future scenarios in 2030 (Y2030) and 2050 (Y2050) (see Figure 1). The database for the current deployments combines information from national datasets, an Europe-wide wind farm database, OpenStreetMap, and the European Marine Observation and Data Network (EMODnet) and was compiled by Fischereit et al. (2025). Besides the location of the wind turbines, the database also contains the turbine type, hub height and rotor diameter, rated power, cut-in and cut-out wind speed, and the turbine power and thrust curves. The Y2030 and Y2050 scenarios consist of a dataset of polygons and installed capacities for the locations of future offshore wind farms provided by the Danish Energy Agency and first analyzed in Hahmann et al. (2025). Every polygon provides the boundary of the development area and a target installed capacity.

For Y2030 we fill the wind farm polygons with the IEA 15 MW wind turbine (Gaertner et al., 2020) with a hub height of 145 m and rotor diameter of 235 m. For Y2050 we use a generic 27 MW wind turbine with a hub height of 180 m and a rotor diameter of 300 m. The 27 MW power and thrust curves were created with PyWake using its thrust and power curve generator (Pedersen et al., 2023).

Every future wind farm polygon is filled with turbine positions using a clustering algorithm to maximise the inter-turbine distances. The algorithm is based on K-means clustering (Lloyd, 1982), where the total number of wind turbines to be placed in the wind farm sets the number of clusters K. The K-means algorithm minimises the within-cluster sum of squares, i.e. the inertia J:

$$J = \sum_{k=1}^{K} \sum_{\mathbf{x}_i \in C_k} \|\mathbf{x}_i - \boldsymbol{\mu}_k\|^2, \tag{1}$$

https://doi.org/10.5194/wes-2026-143
Preprint. Discussion started: 25 August 2026

where C_k denotes the set of points assigned to cluster k, $\mathbf{x}_i$ is a point within that cluster, and $\boldsymbol{\mu}_k$ is the cluster centroid. Upon convergence, the centroid of every cluster provides the wind turbine position $\mathbf{wt}_k = \boldsymbol{\mu}_k$.

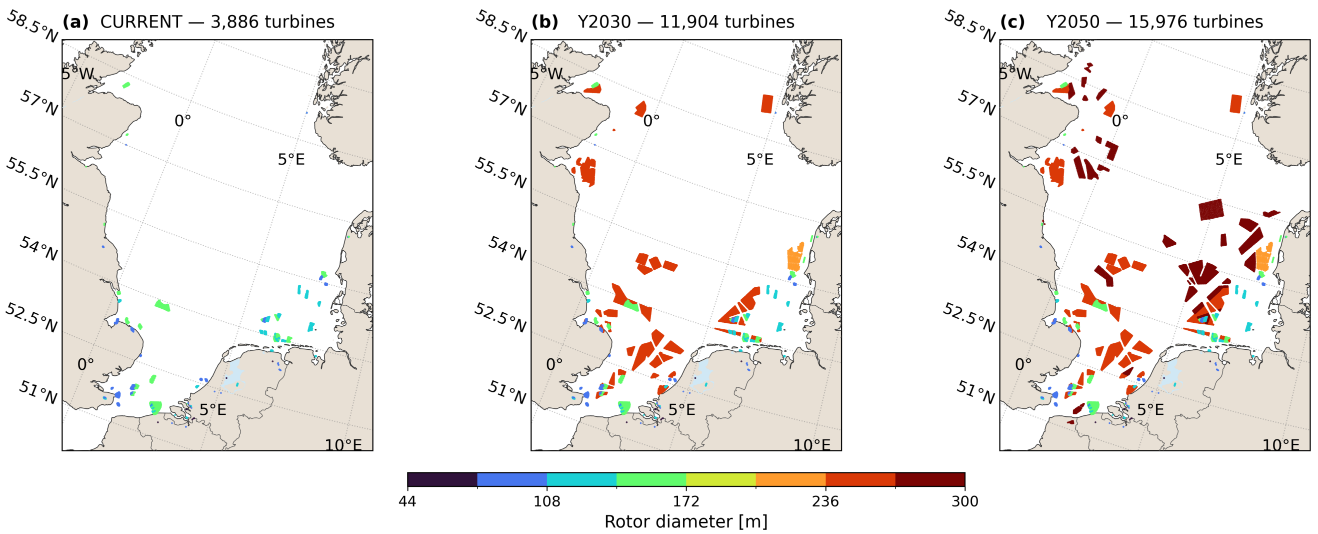

Figure 1. Wind farm scenarios in the study area. The left panel shows the CURRENT scenario (November 2021), the middle panel shows the wind farm scenario for Y2030 and the right panel shows the Y2050 scenario.

2.2 Mesoscale simulation data

The CURRENT, Y2030 and Y2050 scenario simulations were conducted using the WRF model in two configurations: one with the Fitch WFP enabled ($\mathrm{WRF_{Fitch}}$), and one without WFP ($\mathrm{WRF_{NOWF}}$). All simulations are run for the entire meteorological year 2019, which is a single “representative" calendar year, reflecting typical wind energy conditions based on the approach described in Fischereit et al. (2022). In this context, a "representative" year closely matches the long-term climatological distributions of wind speed, wind direction, and atmospheric stability of the region. The simulation domain encompasses the entire North Sea and parts of the Baltic Sea. For further details on the WRF model simulations, see Hahmann et al. (2025).

The quantity extracted from the WRF model output is the yearly-averaged wind speed deficit (U_{deficit}), which is the absolute difference between the $\mathrm{WRF_{NOWF}}$ and $\mathrm{WRF_{Fitch}}$ simulation at 150 m amsl. This specific height is chosen as a compromise between the smaller and taller hub heights in the domain.

https://doi.org/10.5194/wes-2026-143
Preprint. Discussion started: 25 August 2026

3 Methods

3.1 The Wakeness Index WIX

The WIX assesses wake impacts on a regional scale using the wind farm geometry, the wind turbine rotor diameter, and the wind field statistics. It aims to test multiple scenarios to predict wake effects in areas considered for wind energy harvesting, with higher values indicating a greater likelihood of wake influence. The WIX is calculated at every possible turbine position at all the wind direction sectors. The method starts by setting directional rays r over all directions (Fig. 2a), defined as

$$r = \sqrt{(wt_x + R\sin\phi)^2 + (wt_y + R\cos\phi)^2}, \quad (2)$$

where ϕ is the direction from every possible turbine position $wt_{x,y}$; here we choose angular steps of 5° and a distance $R = 100\,\mathrm{km}$ based on extreme wake statistics in some areas of the study region (Platis et al., 2018; Maas and Raasch, 2022). Then, the distances of every ray r are scaled with a rotor diameter scale $s = D/D_{500}$, where D is the turbine diameter of every turbine position $wt_{x,y}$ for the analysed scenario and $D_{500} = 500\,\mathrm{m}$ is an arbitrary turbine diameter bigger than all the available turbines that serves to normalize scenarios.

To account for the wake decay from every turbine, a Gaussian kernel $G(r_{ij}, a, \sigma)$ is applied to weight the rays (Fig. 2b):

$$G(r_{ij}, a, \sigma) = a \exp\left(-\frac{r^2_{scaled}}{2\sigma^2}\right), \quad (3)$$

where r_{ij} is the distance of every point along the scaled distance ray $r_{scaled} = rs$ to the wind turbine, $a = \sqrt{s}$ is the rotor diameter scale factor, and σ is defined as

$$\sigma = \frac{R\,s}{df}, \quad (4)$$

where df is a decay factor further detailed in Section 3.2. The wind direction frequencies are also included as a weighting function in the form of $F(\theta_{ij})$, where θ_{ij} is the wind direction frequency per sector at every turbine position (Fig. 2c). Finally, Figure 2d summarizes the WIX formulation.

We define a preliminary version of the WIX as:

$$\mathrm{WIX} = \sum_{i=1}^{N_y}\sum_{j=1}^{N_x} \rho_{ij} F(\theta_{ij}) G(r_{ij}, a, \sigma). \quad (5)$$

Once the rays and kernels are defined, they are converted to a reference grid through a 2D histogram. The 2D histogram is represented in the WIX by the term $\sum_{i=1}^{N_y}\sum_{j=1}^{N_x}\rho_{ij}$ and provides the spatial density of points on the defined grid and uses the input kernels $F(\theta_{ij})G(r_{ij}, a, \sigma)$ to weight such points. Here, we use a grid spacing of 3 km (same as the WRF model grid) in both the x and y directions. Finally, the point density grid is normalized by its minimum and maximum values to obtain the final WIX.

https://doi.org/10.5194/wes-2026-143
Preprint. Discussion started: 25 August 2026

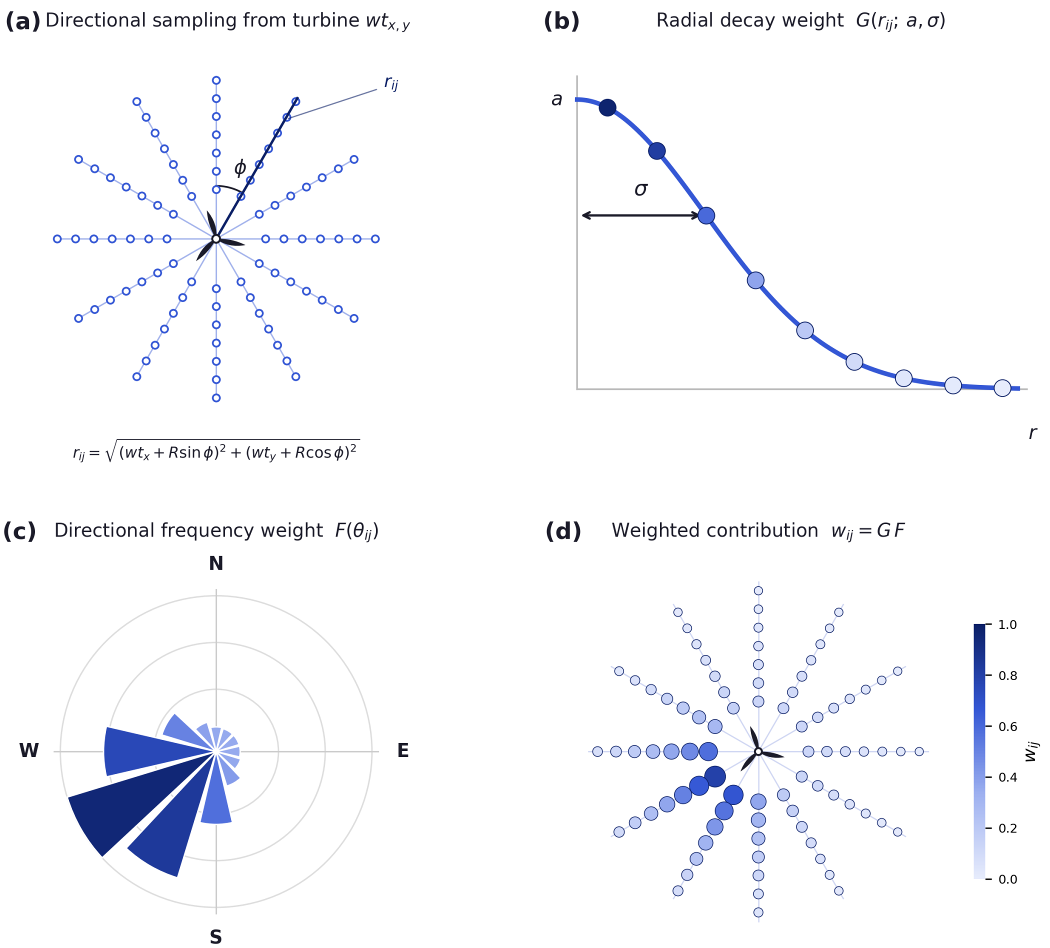

Figure 2. Scheme of the WIX formulation starting from a single turbine position, the ray propagation, and applied kernels.

3.2 Optimisation of the decay factor

To enable the WIX to reproduce climatological NWP-like wind speed deficits, it must incorporate information about how the NWP-derived wake decays with distance. This behavior is captured in the WIX through the decay factor df (Eq. 4). During calibration, a range of decay factors is evaluated against the WRF-derived wind speed deficits to identify the value that optimises one of two objectives (scheme shown in Figure 3): (i) the highest spatial overlap, measured as the intersection-over-union (IoU) between the WIX and WRF-derived wake footprints delineated at the 92, 95, and 98 % wind speed recovery levels; and (ii) the highest coefficient of determination R^2 computed pixel-wise across all grid cells of the domain between the WIX and the normalised WRF-derived wind speed deficit field. An extra pixel-wise calibration is also run, restricted to the Y2030 and Y2050 scenarios, thereby focusing the calibration on the future, higher-density wind farm layouts. The optimisation is carried out in the North Sea and later tested in the Baltic Sea region with the aim of assessing the general applicability of the

https://doi.org/10.5194/wes-2026-143
Preprint. Discussion started: 25 August 2026

optimal df in the calculation of the WIX for other potential regions and wind farm scenarios. The IoU is determined as

$$\mathrm{IoU} = \frac{|A_{\mathrm{WRF}} \cap A_{\mathrm{WIX}}|}{|A_{\mathrm{WRF}} \cup A_{\mathrm{WIX}}|}, \tag{6}$$

where A_{WRF} and A_{WIX} are the wake footprint regions enclosed by a given wind speed recovery iso-line in the WRF and WIX fields, respectively, $|\cdot|$ denotes area, and IoU $\in [0,1]$ (1 = perfect footprint overlap).

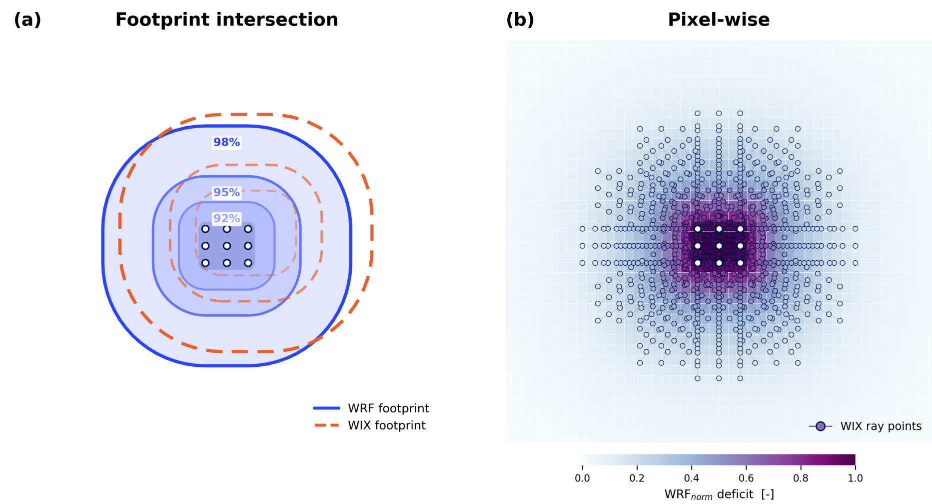

Figure 3. Schematic representation of the calibration objectives. The left panel depicts the first objective maximizing the IoU of the WIX (orange) and WRF (blue) footprint contours, and the right panel shows the second calibration objective maximizing the pixel-wise R^2 between the WIX (ray dots) and WRF model (grid) values. In both panels the white dots in the middle represent wind turbine positions.

4 Results

4.1 Optimisation of the decay factor

The non-dimensional decay factor df was calibrated using two complementary objectives (Table 1). The primary objective maximises the spatial overlap, measured as the intersection-over-union (IoU), between the WIX and WRF wake footprints at the 92, 95, and 98 % wind speed recovery levels; aggregated over all scenarios this yields $df = 2.3$ (mean IoU $= 0.75$), which is adopted as the operating point. A complementary objective maximises the coefficient of determination R^2 computed pixel-wise across all grid cells between the WIX and the normalised WRF wind speed deficit field, giving $df = 1.4$ ($R^2 = 0.79$) over all scenarios; the consistent offset between the footprint and pixel-optimal df reflects the distinction between calibrating for outer wake footprint and for overall wake deficit.

Figure 4 shows the summary of all the calibration objectives. Examined per scenario, the future layouts behave consistently and skilfully: Y2030 and Y2050 share the same footprint optimum ($df = 2.3$, IoU $= 0.84$ and 0.87, respectively) and the same pixel-wise optimum ($df = 1.7$, $R^2 = 0.92$ and 0.88, respectively). The CURRENT scenario, by contrast, optimises at

https://doi.org/10.5194/wes-2026-143
Preprint. Discussion started: 25 August 2026

Open Access
WIND ENERGY SCIENCE
DISCUSSIONS

Table 1. Calibrated decay factor df and corresponding skill metric for each calibration objective and scenario in the North Sea. For each scenario the per-objective optimum is reported (footprint IoU and pixel-wise R^2); the lower block gives the aggregate operating points. The footprint optimum aggregated over all scenarios ($df = 2.3$) is adopted as the operating point.

Scenario	df^* (footprint)	IoU*	df^* (pixel-wise)	R^{2*}
CURRENT	2.0	0.544	1.1	0.620
Y2030	2.3	0.835	1.7	0.924
Y2050	2.3	0.871	1.7	0.882
ALL (footprint)	2.3	0.749	–	–
ALL (domain)	–	–	1.4	0.790
Y2030 & Y2050	–	–	1.7	0.903

a markedly lower df (2.0 for the footprint, 1.1 for the pixel-wise metric) and reaches only IoU $= 0.54$ and $R^2 = 0.62$ even at its own optimum. This discrepancy can be understood by examining the turbine diameter distribution across scenarios (Appendix A1) and sample size: the CURRENT scenario contains considerably fewer turbines than the future scenarios, reducing the statistical robustness of the spatial correlation estimate. Moreover, the CURRENT wind farms exhibit a much narrower range of rotor diameters D than the Y2030 and Y2050 scenarios, and since the WIX depends on the diversity and spread of D values through the rotor diameter scale s, this limits its skill. For these reasons, an extra version of the pixel-wise objective restricts the pixel-wise R^2 to the Y2030 and Y2050 scenarios, focusing on the future, higher-density layouts and yielding $df = 1.7$ ($R^2 = 0.90$).

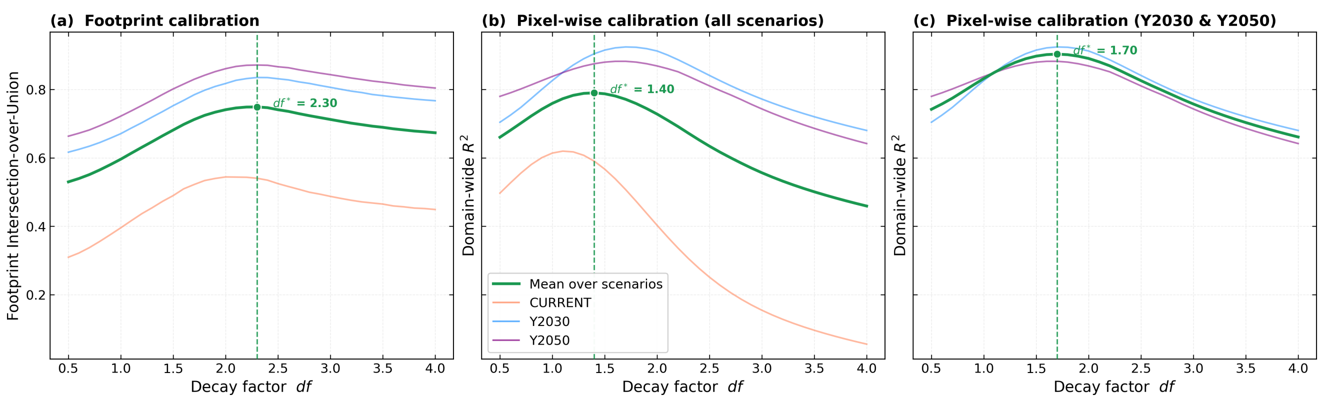

Figure 4. Calibration results for the df parameter under all the wind farm scenarios (see legend). (a) the footprint IoU method vs df, (b) the all-pixel R^2 method for all the scenarios vs df, and (c) the same all-pixel R^2 method vs df only for the future scenarios. The green dashed line marks the optimal decay factor among scenarios.

https://doi.org/10.5194/wes-2026-143
Preprint. Discussion started: 25 August 2026

eawe european academy of wind energy
Open Access WIND ENERGY SCIENCE DISCUSSIONS

4.2 Spatial assessment of all scenarios

Figure 5 illustrates the normalized wind-speed deficit from the WRF model, the corresponding WIX predictions, and the differences between the two for the CURRENT, Y2030, and Y2050 scenarios, computed at the pixel-wise optimum shared by the future layouts ($df = 1.7$). The WIX closely reproduces the spatial structure of the WRF deficit field for the future scenarios, attaining $R^2 = 0.92$ for Y2030 and $R^2 = 0.88$ for Y2050. Since the skill is preserved from Y2030 to Y2050 without any additional tuning, despite the introduction of approximately 4,000 additional turbines and an increase in the maximum rotor diameter to 300 m, we confirm that the WIX generalises across layouts of comparable rotor-diameter range and density. The CURRENT scenario, with far fewer turbines, is reproduced less accurately ($R^2 = 0.62$) and is shown here for completeness. Regarding the differences, the future scenarios show a slight overestimation by the WIX relative to the WRF-derived results is concentrated within the densest German, Dutch, and Norwegian clusters (in blue color in panels f and i), with the surrounding domain near zero; the CURRENT scenario shows correspondingly smaller residuals consistent with its weaker, sparser wakes.

4.3 Evaluation of radial wake transects

We examine the radial structure of the wake recovery by focusing on a case study in the German Bight, a sub-region of the North Sea that hosts wind farms in all three scenarios and therefore allows the WIX to be evaluated as function of the increasing layout density. Radial transects are constructed by binning the WIX and WRF-derived output fields into concentric belts of 10 km spacing centred on the wind farm cluster centroid. Within each annulus in Fig 6 and 7, the azimuthal mean and standard deviation σ_{az} are computed for both the WRF and WIX fields, yielding the mean radial profile and its directional spread as a function of distance from the centroid. The transects are evaluated for two decay factors: the pixel-wise whole-domain optimum ($df = 1.4$) and the future-focused optimum calibrated on the Y2030 and Y2050 scenarios only ($df = 1.7$).

Using the whole-domain $df = 1.4$, the WIX reproduces the WRF-derived radial decay well across all three scenarios, with the mean profiles tracking each other from the near to the far field and the $\pm\sigma_{az}$ spread bands overlapping throughout. Agreement is strongest for the sparse CURRENT layout (RMSE $= 0.024$), where both profiles decay from a normalised deficit of ≈ 0.3 to below 0.1. For this df, the WIX slightly overestimates the deficit in the near and intermediate field of the future scenarios, most visibly for Y2030 (RMSE $= 0.085$), which records the largest error of the three; Y2050, being the densest layout, shows a lower RMSE $= 0.048$ likely due to its broader, more spatially continuous wake field, which produces a smoother radial profile that the WIX captures better.

Increasing the decay factor to the future-focused $df = 1.7$ shifts this balance, as expected from a value calibrated on the higher-density layouts. The error on the future scenarios drops markedly: Y2030 improves to RMSE $= 0.052$ and Y2050 to its best value of RMSE $= 0.028$, with the WIX and WRF-derived mean profiles becoming nearly coincident for Y2050 across the full 0–100 km range and their spread bands almost fully overlapping. This improvement comes at a modest cost for the sparse CURRENT layout, whose RMSE rises from 0.024 to 0.046: with the larger df, the WIX now slightly underestimates the deficit in the near field of the CURRENT layout, reflecting that a decay factor tuned for dense, mutually interacting wakes is marginally too diffusive for an isolated, sparse layout. Taken together, the two cases bracket the trade-off captured by the

https://doi.org/10.5194/wes-2026-143
Preprint. Discussion started: 25 August 2026

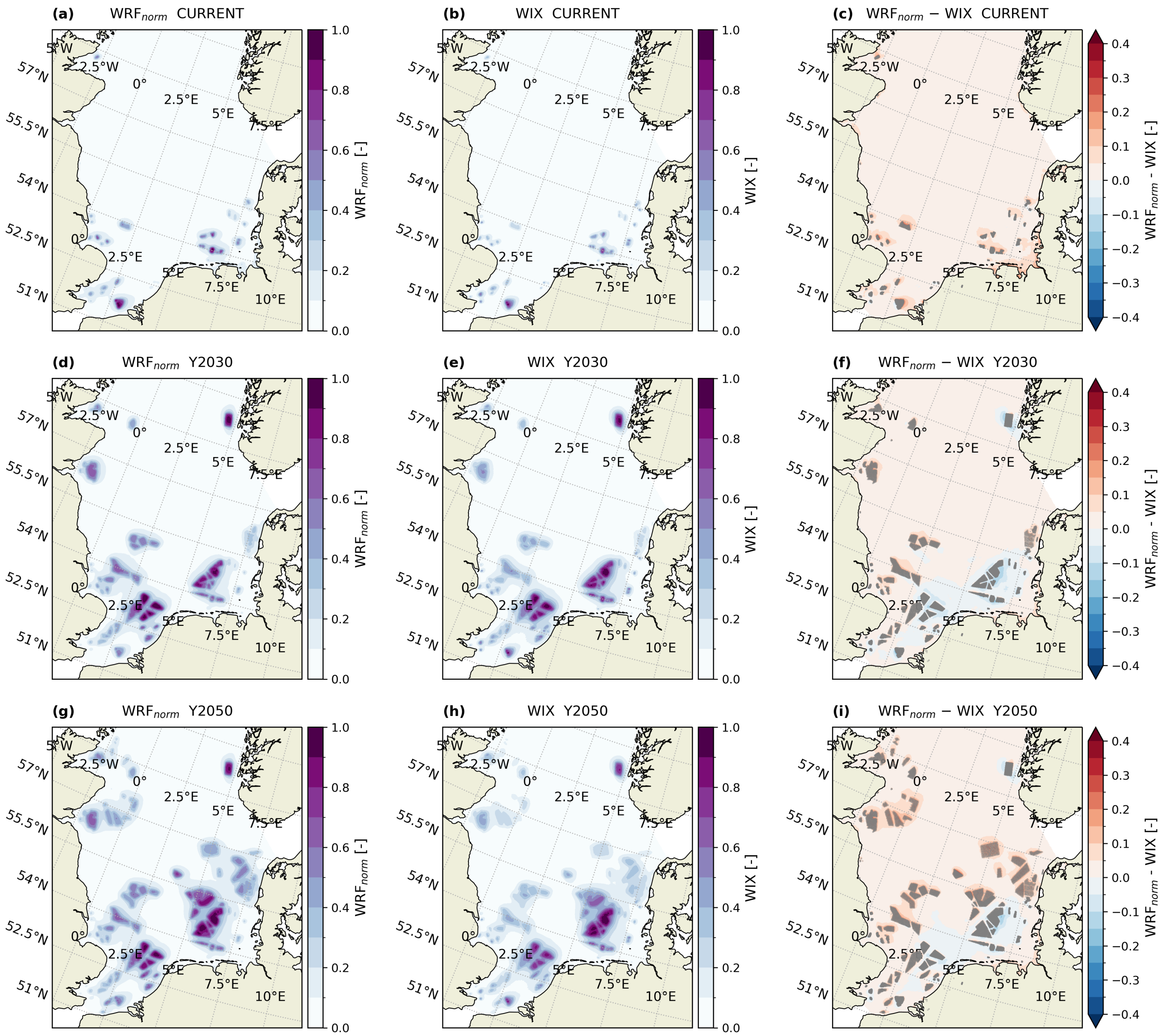

Figure 5. Normalized wind-speed deficit as predicted by the WRF model (a,d,g), the corresponding WIX model predictions (b, e, h), and the differences between the two (c, f, i) for the CURRENT (a–c), Y2030 (d–f), and Y2050 (g–i) scenarios. In (c), (f) and (i), the gray shapes depict the wind farms.

https://doi.org/10.5194/wes-2026-143
Preprint. Discussion started: 25 August 2026

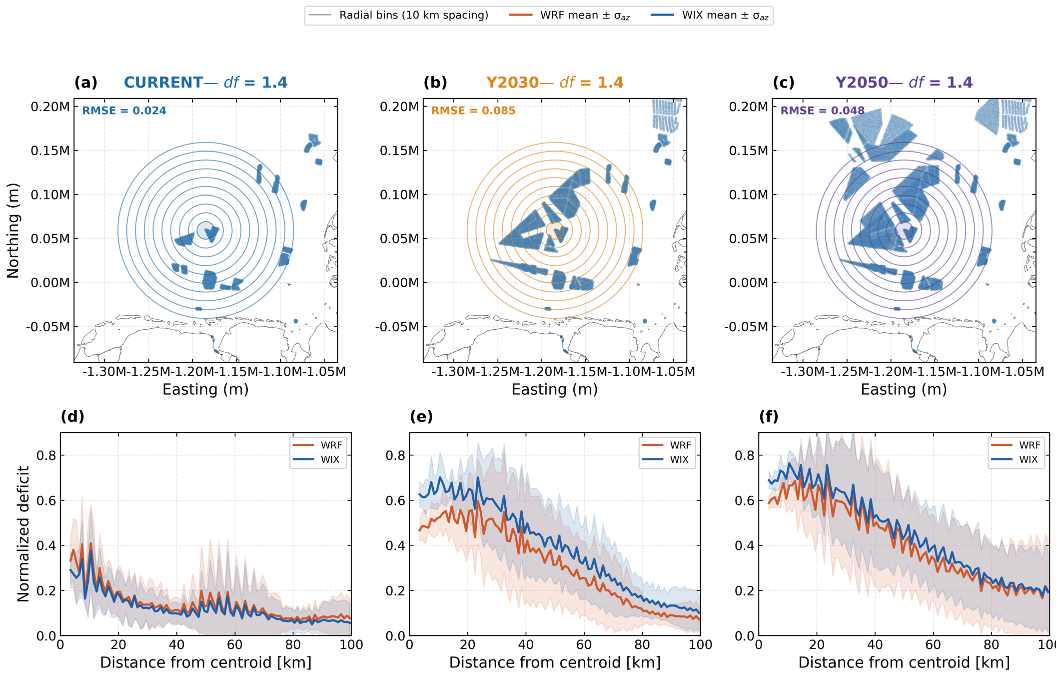

Figure 6. Radial transects of the normalised wind speed deficit for the German Bight case study, for the whole-domain optimum $df = 1.4$. Columns are the CURRENT, Y2030, and Y2050 scenarios. Top row: cluster maps with 10 km radial bins and WRF–WIX RMSE annotated. Bottom row: azimuthally averaged deficit versus distance from the centroid for WRF (orange) and WIX (blue) with $\pm\sigma_{az}$ bands.

calibration objectives: $df = 1.4$ balances all scenarios, whereas $df = 1.7$ optimises the future, higher-density layouts that are the primary target of the assessment, with the German Bight transects confirming that either choice yields physically consistent radial recovery across a four-fold change in turbine density.

4.4 Regional wake footprint assessment

Capturing the footprint associated with different wake-recovery rates is a central objective of the WIX, and accurately predicting these footprints across recovery levels is crucial for our analysis. Figure 8 compares the WIX and the normalized WRF-derived wind speed deficit at three wind speed recovery thresholds, 92%, 95%, and 98%, computed at the footprint operating point ($df = 2.3$). These thresholds are defined from the WRF-derived wind speed deficit, and the corresponding WIX iso-lines are extracted accordingly. The future scenarios, which share the same footprint optimum (IoU $= 0.84$ for Y2030 and 0.87 for Y2050), both reproduce the WRF-derived footprints closely across all three recovery levels, with Y2050 in slightly better agreement, consistent with its broader and more spatially continuous wakes. The CURRENT scenario is shown in Appendix B1.

https://doi.org/10.5194/wes-2026-143
Preprint. Discussion started: 25 August 2026

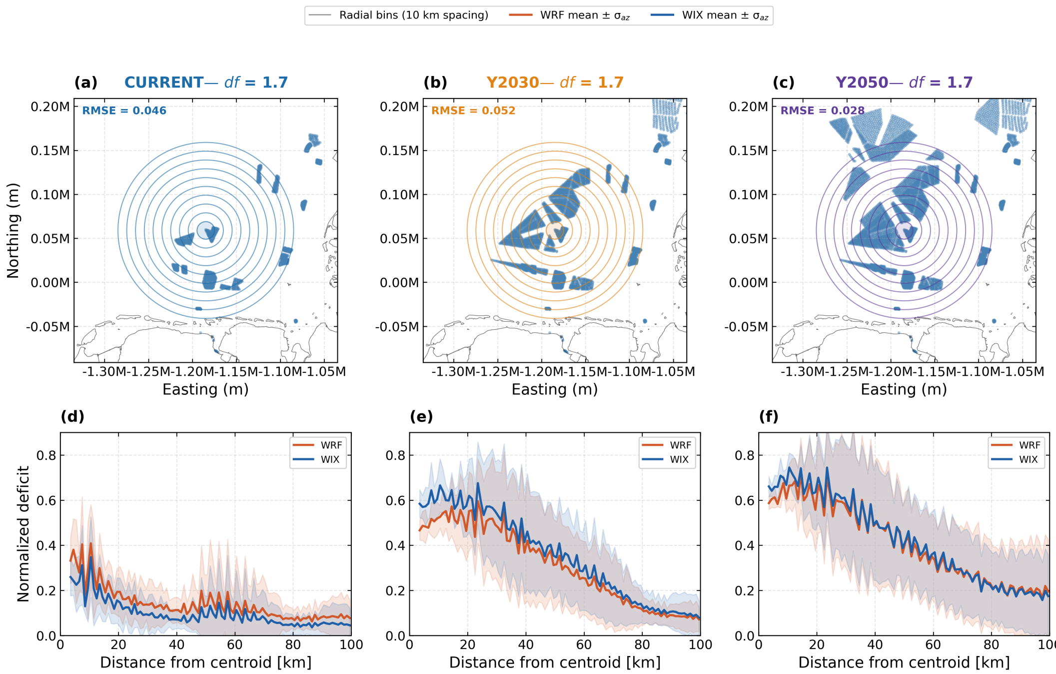

Figure 7. Radial transects of the normalised wind speed deficit for the German Bight case study, for the future-focused optimum $df = 1.7$. Columns are the CURRENT, Y2030, and Y2050 scenarios. Top row: cluster maps with 10 km radial bins and WRF–WIX RMSE annotated. Bottom row: azimuthally averaged deficit versus distance from the centroid for WRF (orange) and WIX (blue) with $\pm\sigma_{az}$ bands.

4.5 Atmospheric regime dependency: WIX performance in the Baltic Sea

Evaluating the WIX in a region with a different atmospheric climatology is essential for assessing its geographical transferability. The Baltic Sea provides a compelling test case for this purpose, as its atmospheric stratification is climatologically more stable than in the North Sea: stable atmospheric episodes there tend to be longer, more intense, and more prevalent during the spring and summer months (Svensson et al., 2016), which in turn promotes the persistence of wind farm wakes. Under stable stratification, suppressed vertical turbulent mixing limits momentum entrainment into the wake, resulting in slower recovery and more extended velocity deficit footprints downstream compared to neutral or convective conditions (Abkar and Porté-Agel, 2015; Platis et al., 2018). In contrast, the North Sea experiences neutral conditions more frequently, driven by higher mean wind speeds and smaller air-sea temperature gradients (Sathe et al., 2011). These contrasting stability characteristics make the two regions particularly well-suited for a comparative evaluation of the WIX.

In this case (Figure 9), the WIX is evaluated in a region with wind farms not used during its calibration, namely the Baltic Sea under the Y2050 scenario, using the operating-point decay factor calibrated in the North Sea. To quantify the sensitivity of the result to the calibration region, the figure also shows, as a shaded purple band, the difference between the WIX footprint computed with the North Sea optimum and that computed with a decay factor recalibrated on the Baltic Sea. This band is

https://doi.org/10.5194/wes-2026-143
Preprint. Discussion started: 25 August 2026

WIND ENERGY SCIENCE DISCUSSIONS

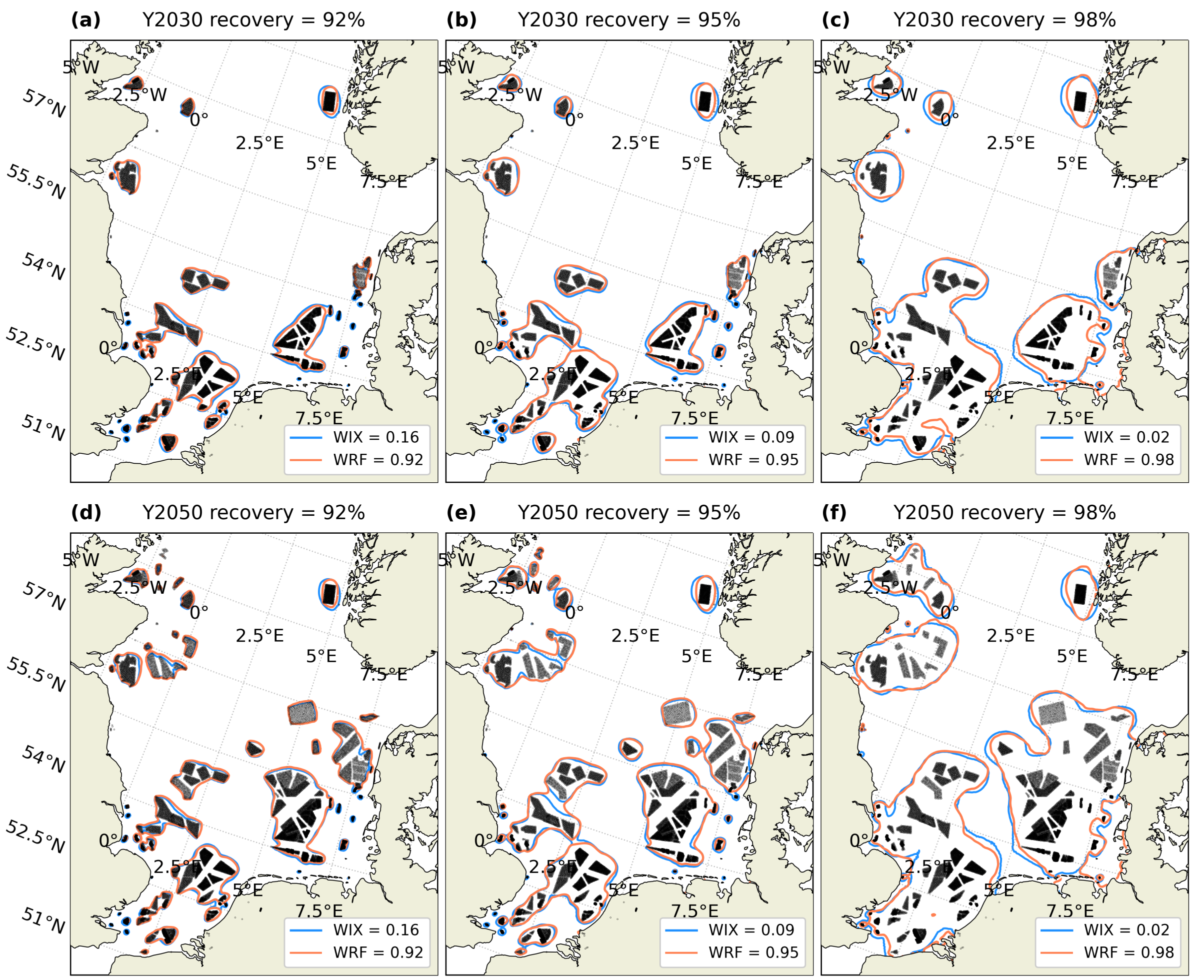

Figure 8. Wind speed deficit footprints at 92% (a), 95% (b), and 98% (c) recovery rates for the Y2030 (a–c) and Y2050 (d–f) scenarios. The orange contours show the WRF-derived wind speed deficit, and the blue contours show the corresponding WIX values. The black dots show the wind turbine positions.

https://doi.org/10.5194/wes-2026-143
Preprint. Discussion started: 25 August 2026

Open Access
WIND ENERGY SCIENCE
DISCUSSIONS

almost negligible across the domain, confirming that the North Sea decay factor transfers to the Baltic without meaningful loss of accuracy; the largest difference appears south of Sweden at the 98% recovery level, where the more extended far-wake footprint is most sensitive to the choice of df. Overall, the WIX demonstrates comparable performance to that observed in the North Sea, successfully capturing the wake footprint of the majority of wind farms. The main exception, where the WIX underperforms, occurs for smaller and less dense wind farms south of Lolland, close to Fehmarn Island, where the WIX moderately overestimates the extent of the wake. Appendix C1 shows the optimal metrics in this region.

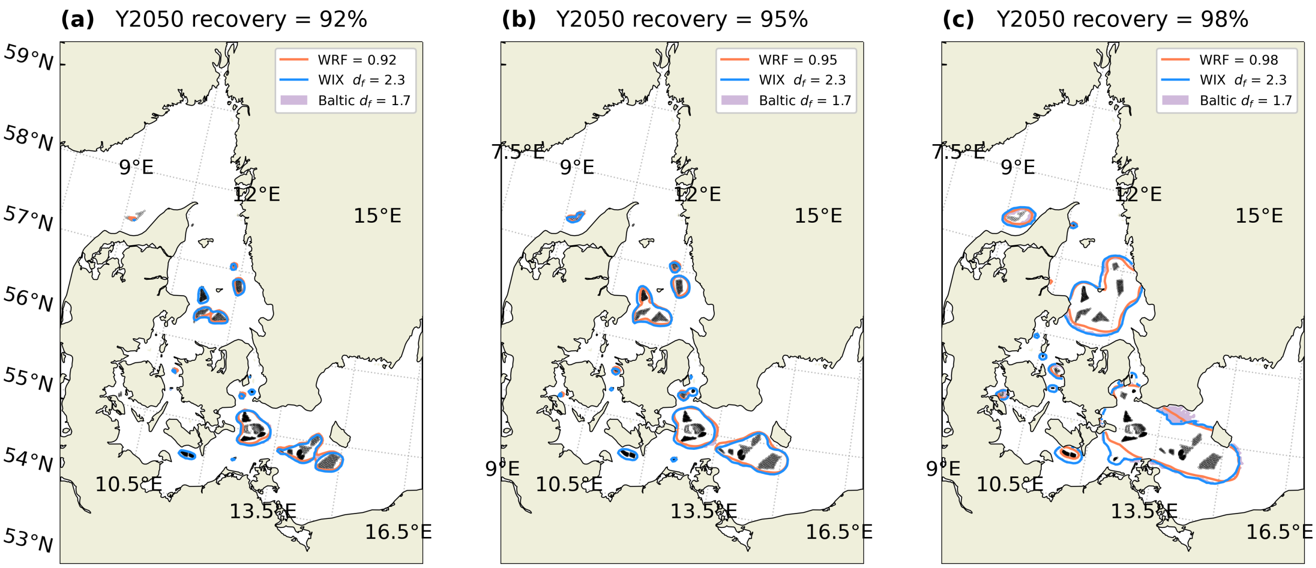

Figure 9. Wind speed deficit footprints at 92% (a), 95% (b), and 98% (c) recovery rates for the Y2050 scenario. The orange contours show the WRF wind speed deficit, and the blue contours show the corresponding WIX values. The black dots show the wind turbine positions.

4.6 Regional wake footprint assessment: NEWA implementation

So far the WIX has been computed using wind direction frequencies derived from the WRF simulations described in Section 2.2. For the WIX to be applicable independently, an external climatological data source is needed. The New European Wind Atlas (NEWA; Hahmann et al., 2020; Dörenkämper et al., 2020) dataset provides 30-year wind direction frequency climatologies across Europe and represents a suitable candidate for this purpose. Figure 10 compares three quantities at the 95% wind speed recovery threshold for all scenarios: the WRF-derived wind speed deficit, the WIX computed with the WRF wind direction frequencies of Sect. 2.2, and the WIX computed with the NEWA wind direction frequencies. The two WIX estimates are in near-perfect agreement, showing that the NEWA and WRF wind direction frequencies are effectively interchangeable for this purpose. Any other trusted dataset providing direction frequency information could be used in the same way.

https://doi.org/10.5194/wes-2026-143
Preprint. Discussion started: 25 August 2026

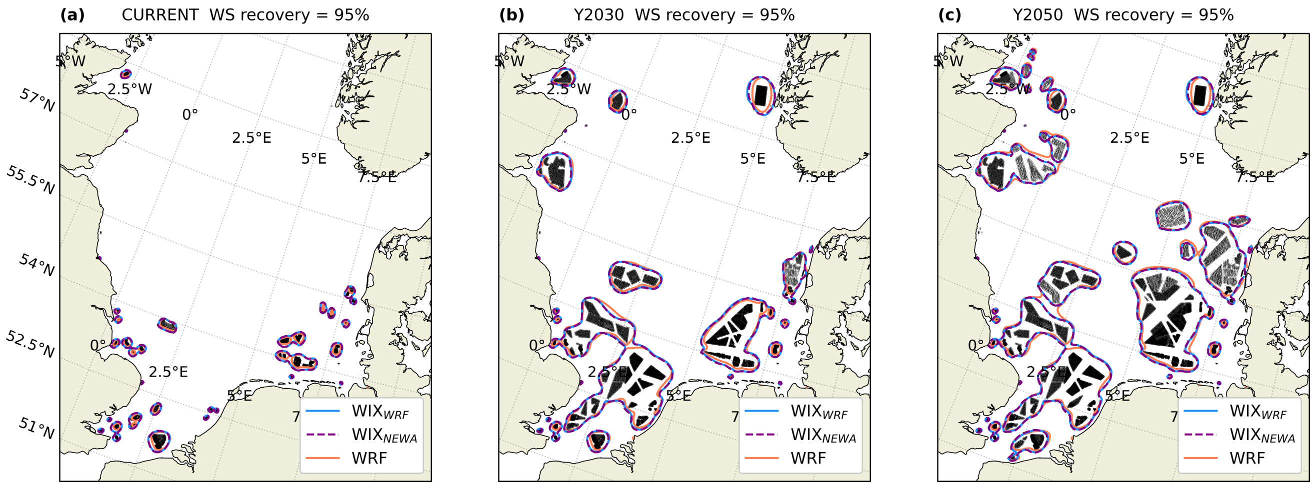

Figure 10. Wind speed deficit footprints at 95% recovery rates for the CURRENT (a), Y2030 (b) and Y2050 (c) scenarios. The orange contours show the WRF-derived wind speed deficit, the blue contours show the corresponding WIX values based on the wind direction frequency from WRF from Sect. 2.2, and the purple contours depict the WIX based on the wind direction frequency from NEWA. The black dots show the wind turbine positions.

4.7 Pre-feasibility assessment: WIX applied to hypothetical wind farm clusters

To illustrate the potential of the WIX as a pre-feasibility planning tool, we apply it to three hypothetical wind farm clusters for which no reference wind speed deficit data exist. The WIX is computed using the WRF wind direction frequencies from Sect. 2.2 under the Y2030 scenario. Rather than a quantitative validation, the aim here is to demonstrate how the WIX can provide rapid, qualitative insight into the expected wake footprint prior to any detailed flow modelling. The three scenarios considered are: a large offshore cluster situated in the central North Sea (Scenario 1), a nearshore cluster off the coast of Great Britain (Scenario 2), and a cluster located in the German Bight (Scenario 3). Figure 11 shows the resulting WIX fields for each scenario. The spatial patterns reflect the dominant wind direction climatology of each region, with the wake footprints extending in directions consistent with the prevailing winds. These results suggest that the WIX can provide physically meaningful and regionally coherent wake footprint estimates in planning contexts where observational or high-resolution simulation data are not yet available, supporting its use as a lightweight screening tool in the early stages of wind farm site assessment.

5 Discussion and limitations

The results indicate that the skill of the WIX in reproducing the WRF-derived wake fields scales with the number of turbines within a layout. Denser scenarios provide a richer set of weighted ray points from which the WIX field is constructed, allowing the WIX to capture wake footprints more faithfully. This dependence appears for the two cases where the WIX slightly underperforms, the sparse CURRENT scenario and the Baltic Sea region, both of which are characterised by relatively few turbines.

https://doi.org/10.5194/wes-2026-143
Preprint. Discussion started: 25 August 2026

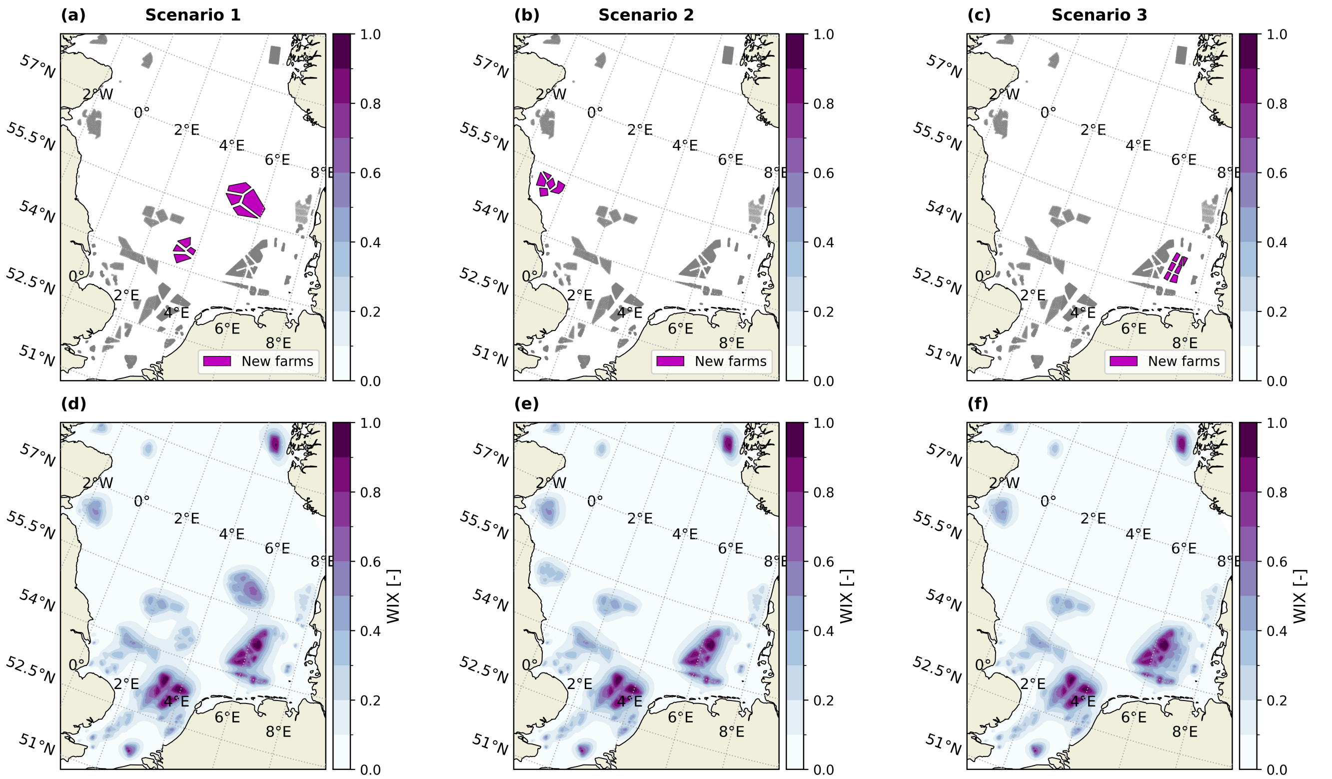

Figure 11. WIX applied to three hypothetical wind farm clusters: (a) central North Sea (Scenario 1), (b) coast of Great Britain (Scenario 2), and (c) German Bight (Scenario 3). (a–c) hypothetical wind farm layouts (magenta). (d–f) corresponding WIX fields.

With fewer data points, the two-dimensional histogram that bins the spatial rays by density becomes noisier, and the resulting WIX field cannot reach the high correlations achieved for the data-rich Y2030 and Y2050 scenarios. The number and diversity of turbines therefore set a practical lower bound on the robustness of the WIX, below which the binning step is too sparsely populated to yield a stable footprint.

Another dependence is on the atmospheric regime. The optimal decay factor is region-specific: the Baltic Sea yields a lower value of the *df* optimum than the North Sea, corresponding to slightly longer wakes, which is physically consistent with the more frequent and intense stable conditions of that basin, where reduced vertical mixing extends the wake recovery distance. Irrespectively, this shift in the value of *df* has only a minor effect on the footprint delineation, so a decay factor transferred from the North Sea still captures the Baltic Sea wakes well; nonetheless, in atmospheric regimes that differ substantially from the calibration region, recalibration of the decay factor against locally representative output remains advisable.

Moreover, since the Y2030 and Y2050 scenarios share the same *df* optima, despite the differences in the amount of installed turbines between them, the WIX demonstrates generalizability across layouts spanning a comparable range of rotor diameters and turbine densities. This is a key strength for forward-looking assessments, as a single decay factor calibrated on present-day

https://doi.org/10.5194/wes-2026-143
Preprint. Discussion started: 25 August 2026

eawe european academy of wind energy
Open Access WIND ENERGY SCIENCE DISCUSSIONS

or near-future layouts can be applied to denser future scenarios without recalibration, provided the turbine population remains within a similar range.

A further consequence of the WIX's low computational cost is the speed at which it can be recalibrated. Because a full calibration takes only a fraction of the time of the reference simulations, the WIX can be re-tuned almost instantly whenever newer or alternative NWP simulations become available. This is a relevant asset given the ongoing debate on the accuracy of WFPs, which do not fully capture the details of the wakes that are also important for regional analysis (Radünz et al., 2025; García-Santiago et al., 2026). As WFPs continue to improve, the WIX can be re-tuned against the most recent reference simulations at negligible cost, ensuring that its footprint estimates track the current state of the art rather than being fixed to a single parameterisation.

6 Conclusions

In this work, we showcase the WIX, a geometry-based indicator designed to provide rapid, first-order estimates of climatological wind farm wake footprints. The WIX requires only three inputs: turbine coordinates and rotor diameters, wind direction frequency statistics, and a single tuneable decay factor df. WIX is intended as a lightweight screening tool for multi-scenario wind farm planning prior to committing to full NWP simulations.

The df value was calibrated against WRF-simulated wind speed deficits using two complementary objectives. The primary objective maximises the footprint IoU between the WIX and WRF wake footprints at the 92, 95, and 98 % wind speed recovery iso-lines: aggregated over all scenarios this yields $df = 2.3$ (mean IoU $= 0.75$), adopted as the operating point. The second objective maximises the coefficient of determination R^2 computed pixel-wise across all grid cells over all the scenarios, giving $df = 1.4$ ($R^2 = 0.79$). The offset between the two objectives reflects the distinction between calibrating for wake extent and for wind speed deficit magnitude. Restricting this same pixel-wise objective to the future Y2030 and Y2050 scenarios yields $df = 1.7$ ($R^2 = 0.90$). The choice among these optima is application-dependent, and their spread provides a practical measure of the uncertainty in the WIX wake footprint.

The future layouts behave consistently and skilfully, with Y2030 and Y2050 sharing the same footprint optimum ($df = 2.3$, IoU $= 0.84$ and 0.87) and pixel-wise optimum ($df = 1.7$, $R^2 = 0.92$ and 0.88). Since they share their optima despite the large increase in installed turbines, we demonstrate the generalizability of the WIX across layouts of comparable rotor-diameter range and density. The CURRENT scenario, by contrast, optimises at a markedly lower df value (2.0 for the footprint, 1.1 for the pixel-wise objective) and reaches only IoU $= 0.54$ and $R^2 = 0.62$ even at its own optimum. This traces to its fewer turbines and narrower diversity of rotor diameters: with fewer sampling points, the two-dimensional histogram that bins the spatial rays by density becomes noisier, so the density and diversity of turbines set an initial boundary on the applicability of the tool.

The WIX was validated in the Baltic Sea using the North Sea df value, with all calibrated parameters held static. Despite the more frequent stable atmospheric episodes of that basin, it captured the wake footprint of most wind farms without region-specific tuning (shown for Y2050, which encompasses all preceding scenarios). A recalibration on the Baltic yields a slightly lower df value, marginally longer wakes, consistent with the reduced vertical mixing of a more stable regime, but with only

eawe european academy of wind energy
Open Access WIND ENERGY SCIENCE DISCUSSIONS

a minor effect on the delineated footprint, confirming that a *df* can be transferred across sea basins within the range of turbines studied. A moderate overestimation of the wake extension was observed for smaller wind farms south of Lolland, near Fehmarn, suggesting that capacity density may influence WIX performance in near-wake regions. In weather regimes that differ substantially from the North Sea in terms of atmospheric stability statistics, recalibration of the *df* value remains advisable.

The wind direction frequency climatologies required as input can be sourced externally, removing the dependency on WRF outputs. The near-perfect agreement between WIX estimates using WRF-derived and NEWA-derived wind direction frequencies shows that reliable wind climatologies from other datasets can be used as input for the WIX.

A key practical advantage of the WIX is its computational efficiency: wake footprints over the whole North Sea are generated in seconds on 32 CPUs, compared to the CPU-weeks required when performing climatological simulations with the WRF model over extended regions. The WIX is therefore well-suited for rapid screening of layouts and turbine configurations in early site assessment, where full NWP runs are not yet warranted. Application to three hypothetical wind farm clusters in the North Sea (Section 4.7) demonstrates its potential as a pre-feasibility planning tool, producing wake footprints that are statistically meaningful and consistent with each region's prevailing wind direction climatology.

Code and data availability. The code and atmospheric datasets associated with this article are available at https://doi.org/10.11583/DTU.33162212 together with North Sea and Baltic Sea wind farm layout files including the CURRENT, Y2030 and Y2050 wind farm scenarios. The exact version of the CURRENT scenario used in the NWP simulations is not publicly available at the moment; therefore, we replaced those turbine values with a similar, publicly available version of the CURRENT scenario available at https://doi.org/10.5281/zenodo.17495820. The turbine positions in the CURRENT scenario remain identical; however, the turbine rotor diameter values vary by on the order of 1.5 m on average, so results in these areas may differ slightly from those in this article.

https://doi.org/10.5194/wes-2026-143
Preprint. Discussion started: 25 August 2026

Open Access
WIND ENERGY SCIENCE DISCUSSIONS

Appendix A: Turbine diameter D statistics per wind farm scenario.

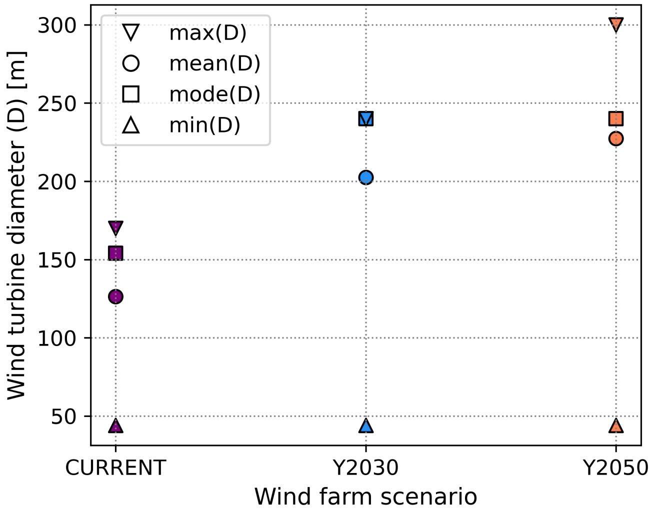

Figure A1. Statistics of the turbine diameter D across scenarios. The x axis shows all the scenarios considered in this study and the y axis displays the respective turbine diameter statistics. The purple markers represent the CURRENT scenario statistics, the blue markers represent the Y2030 and the orange markers represent the Y2050 scenario.

https://doi.org/10.5194/wes-2026-143
Preprint. Discussion started: 25 August 2026

Appendix B: Wake footprints of the CURRENT scenario

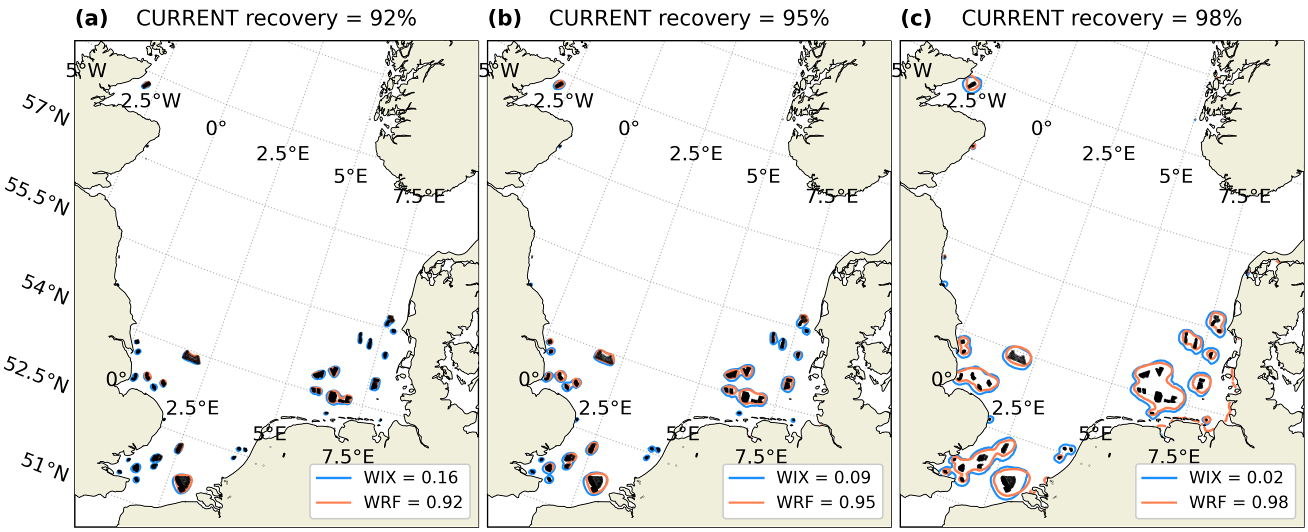

Figure B1. Wind speed deficit footprints at 92% (a), 95% (b), and 98% (c) recovery rates for the CURRENT scenario. The orange contours show the WRF-derived wind speed deficit, and the blue contours show the corresponding WIX values. The black dots show the wind turbine positions.

Appendix C: Calibration metrics in the Baltic Sea

Table C1. Calibrated decay factor d_f and corresponding skill metric for each calibration objective and scenario in the Baltic Sea. For each scenario the per-objective optimum is reported (footprint IoU and pixel-wise R^2); the lower block gives the aggregate operating points. The footprint optimum aggregated over all scenarios ($d_f = 1.7$) is adopted as the operating point.

	df^* (footprint)	IoU*	df^* (pixel-wise)	R^{2*}
CURRENT	1.3	0.338	1.3	0.435
Y2030	1.7	0.791	1.7	0.884
Y2050	1.9	0.782	1.6	0.869
ALL (footprint)	1.7	0.636	–	–
ALL (domain)	–	–	1.5	0.722
Y2030 & Y2050	–	–	1.6	0.876

https://doi.org/10.5194/wes-2026-143
Preprint. Discussion started: 25 August 2026

Author contributions. NA conceptualised the study, developed the methodology, carried out the analysis, and wrote the first draft. AH performed the NWP simulations and contributed to reviewing and editing the manuscript. AP provided feedback on the conception of the study and the analysis, and reviewed the manuscript.

Competing interests. Co-authors AH and AP are editors of the Wind Energy Science journal.

Acknowledgements. We acknowledge the support of the Independent Research Fund Denmark funding through the Multi-scale Atmospheric Modeling Above the Seas (MAMAS) project (no. 0217-00055B), the EU Horizon Europe project WIMBY (Grant Agreement No. 101083460), and the Technical University of Denmark (DTU). The authors gratefully acknowledge the computational and data resources provided on the Sophia HPC Cluster at the Technical University of Denmark, DOI: 10.57940/FAFC-6M81. AI tools were used to improve the text readability of some sections and to clean the code for plotting some of the results.

https://doi.org/10.5194/wes-2026-143
Preprint. Discussion started: 25 August 2026

References

Abkar, M. and Porté-Agel, F.: Influence of atmospheric stability on wind-turbine wakes: A large-eddy simulation study, Physics of Fluids, 27, 035 104, https://doi.org/10.1063/1.4913695, _eprint: https://pubs.aip.org/aip/pof/article-pdf/doi/10.1063/1.4913695/15919392/035104_1_online.pdf, 2015.

Allaerts, D. and Meyers, J.: Sensitivity and feedback of wind-farm-induced gravity waves, Journal of Fluid Mechanics, 862, 990–1028, https://doi.org/10.1017/jfm.2018.969, 2019.

Alonso-De-Linaje, N. G., Hahmann, A. N., and Peña, A.: Towards a regional wind farm planning approach: The Wakeness Index, Journal of Physics: Conference Series, 3016, 012 050, https://doi.org/10.1088/1742-6596/3016/1/012050, 2025.

Bastankhah, M. and Porté-Agel, F.: A new analytical model for wind-turbine wakes, Renewable Energy, 70, 116–123, https://doi.org/10.1016/j.renene.2014.01.002, 2014.

Borgers, R., Dirksen, M., Wijnant, I. L., Stepek, A., Stoffelen, A., Akhtar, N., Neirynck, J., Walle, J. d., Meyers, J., and Lipzig, N. P. M. v.: Mesoscale modelling of North Sea wind resources with COSMO-CLM: model evaluation and impact assessment of future wind farm characteristics on cluster-scale wake losses, Wind Energy Science, 9, 697–719, https://doi.org/10.5194/wes-9-697-2024, 2024.

Calaf, M., Meneveau, C., and Meyers, J.: Large eddy simulation study of fully developed wind-turbine array boundary layers, Physics of Fluids, 22, https://doi.org/10.1063/1.3291077, 2010.

Dörenkämper, M., Olsen, B. T., Witha, B., Hahmann, A. N., Davis, N. N., Barcons, J., Ezber, Y., Garcia-Bustamante, E., González-Rouco, J. F., Navarro, J., Sastre-Marugán, M., Sīle, T., Trei, W., Žagar, M., Badger, J., Gottschall, J., Rodrigo, J. S., and Mann, J.: The Making of the New European Wind Atlas – Part 2: Production and evaluation, Geoscientific Model Development, 13, 5079–5102, https://doi.org/10.5194/gmd-13-5079-2020, 2020.

Elizalde, A., Akhtar, N., Geyer, B., and Schrum, C.: Uncertainty in North Sea offshore wind power: contributions of reanalysis forcing, turbine type, and wake parameterization, Wind Energy Science, 11, 1077–1095, https://doi.org/10.5194/wes-11-1077-2026, 2026.

Fischereit, J., Imberger, M., and Larsén, X. G.: Cost-effective mesoscale modeling methods for offshore wind resource assessment with farm wake effect, in: WindEurope Technology Workshop 2022 : Resource Assessment and Analysis of Operating Wind Farms, https://windeurope.org/tech2022/, 2022.

Fischereit, J., Olsen, B. T. E., Imberger, M., Vedel, H., Møller, K. H., Hahmann, A. N., and Larsén, X. G.: Modelling wind farm effects in HARMONIE-AROME (cycle 43.2.2) – part 2: Wind turbine database and application to Europe, https://doi.org/10.5194/egusphere-2025-5407, 2025.

Fitch, A. C., Olson, J. B., Lundquist, J. K., Dudhia, J., Gupta, A. K., Michalakes, J., and Barstad, I.: Local and Mesoscale Impacts of Wind Farms as Parameterized in a Mesoscale NWP Model, Monthly Weather Review, 140, 3017 – 3038, https://doi.org/10.1175/MWR-D-11-00352.1, 2012.

Frandsen, S.: On the wind speed reduction in the center of large clusters of wind turbines, Journal of Wind Engineering and Industrial Aerodynamics, 39, 251–265, https://doi.org/10.1016/0167-6105(92)90551-K, 1992.

Gaertner, E., Rinker, J., Sethuraman, L., Zahle, F., Anderson, B., Barter, G., Abbas, N., Meng, F., Bortolotti, P., Skrzypinski, W., Scott, G., Feil, R., Bredmose, H., Dykes, K., Sheilds, M., Allen, C., and Viselli, A.: Definition of the IEA 15-Megawatt Offshore Reference Wind Turbine, Tech. rep., International Energy Agency, https://www.nrel.gov/docs/fy20osti/75698.pdf, 2020.

García-Santiago, O., Badger, J., Hahmann, A. N., Volker, P. J. H., Ott, S., Van Der Laan, M. P., and Kelly, M.: A wind-farm wake-turbulence parameterization for the WRF model (EWP v2.0), https://doi.org/10.5194/egusphere-2026-2144, 2026.

https://doi.org/10.5194/wes-2026-143
Preprint. Discussion started: 25 August 2026

WIND ENERGY SCIENCE DISCUSSIONS

Hahmann, A. N., Sīle, T., Witha, B., Davis, N. N., Dörenkämper, M., Ezber, Y., García-Bustamante, E., González-Rouco, J. F., Navarro, J., Olsen, B. T., and Söderberg, S.: The making of the New European Wind Atlas – Part 1: Model sensitivity, Geoscientific Model Development, 13, 5053–5078, https://doi.org/10.5194/gmd-13-5053-2020, 2020.

Hahmann, A. N., Imberger, M., Fischereit, J., Alonso-de Linaje, N. G., and Badger, J.: Environmental Mapping and Screening of the Offshore Wind Potential in Denmark: Sensitivity mapping: Wind, Tech. rep., DTU Wind and Energy Systems, https://orbit.dtu.dk/files/400503926/ENSreport_V4.0_1May2025.pdf, 2025.

Lloyd, S.: Least squares quantization in PCM, IEEE Transactions on Information Theory, 28, 129–137, https://doi.org/10.1109/TIT.1982.1056489, 1982.

Lundquist, J. K., DuVivier, K. K., Kaffine, D., and Tomaszewski, J. M.: Costs and consequences of wind turbine wake effects arising from uncoordinated wind energy development, Nature Energy, 4, 26–34, https://doi.org/10.1038/s41560-018-0281-2, 2018.

Ma, Y., Archer, C. L., and Vasel-Be-Hagh, A.: The Jensen wind farm parameterization, Wind Energy Science, 7, 2407–2431, https://doi.org/10.5194/wes-7-2407-2022, 2022.

Maas, O. and Raasch, S.: Wake properties and power output of very large wind farms for different meteorological conditions and turbine spacings: a large-eddy simulation case study for the German Bight, Wind Energy Science, 7, 715–739, https://doi.org/10.5194/wes-7-715-2022, 2022.

Pedersen, M. M., Forsting, A. M., Laan, P. v. d., Riva, R., Romàn, L. A. A., Risco, J. C., Friis-Møller, M., Quick, J., Christiansen, J. P. S., Rodrigues, R. V., Olsen, B. T., and Réthoré, P.-E.: PyWake 2.5.0: An Open-Source Wind Farm Simulation Tool, https://gitlab.windenergy.dtu.dk/TOPFARM/PyWake, 2023.

Platis, A., Siedersleben, S. K., Bange, J., Lampert, A., Bärfuss, K., Hankers, R., Cañadillas, B., Foreman, R., Schulz-Stellenfleth, J., Djath, B., Neumann, T., and Emeis, S.: First in situ evidence of wakes in the far field behind offshore wind farms, Scientific Reports, 8, 2163, https://doi.org/10.1038/s41598-018-20389-y, 2018.

Radünz, W. C., Kasper, J. H., Stevens, R. J. A. M., and Lundquist, J. K.: Under-resolved gradients: slow wake recovery and fast turbulence decay with mesoscale Wind Farm Parameterizations, https://doi.org/10.5194/wes-2025-147, 2025.

Sathe, A., Gryning, S.-E., and Peña, A.: Comparison of the atmospheric stability and wind profiles at two wind farm sites over a long marine fetch in the North Sea, Wind Energy, 14, 767–780, https://doi.org/10.1002/we.456, 2011.

Skamarock, W. C., Klemp, J. B., Dudhia, J., Gill, D. O., Liu, Z., Berner, J., Wang, W., Powers, J. G., Duda, M. G., Barker, D. M., and Huang, X.-Y.: A Description of the Advanced Research WRF Model Version 4, Tech. rep., NSF National Center for Atmospheric Research, https://doi.org/10.5065/1DFH-6P97, 2019.

Svensson, N., Bergström, H., Sahlée, E., and Rutgersson, A.: Stable atmospheric conditions over the Baltic Sea: model evaluation and climatology, BOREAL ENVIRONMENT RESEARCH, https://doi.org/https://doi.org/10.60910/9htk-pxwb, 2016.

van der Laan, M. P., García-Santiago, O., Kelly, M., Forsting, A. M., Dubreuil-Boisclair, C., Seim, K. S., Imberger, M., Peña, A., Sørensen, N. N., and Réthoré, P.-E.: A new RANS-based wind farm parameterization and inflow model for wind farm cluster modeling, Wind Energy Science, 8, 819–848, https://doi.org/10.5194/wes-8-819-2023, 2023.

Volker, P. J. H., Badger, J., Hahmann, A. N., and Ott, S.: The Explicit Wake Parametrisation V1.0: a wind farm parametrisation in the mesoscale model WRF, Geoscientific Model Development, 8, 3715–3731, https://doi.org/10.5194/gmd-8-3715-2015, 2015.

Warder, S. C. and Piggott, M. D.: The future of offshore wind power production: Wake and climate impacts, Applied Energy, 380, 124 956, https://doi.org/10.1016/j.apenergy.2024.124956, 2025.

https://doi.org/10.5194/wes-2026-143
Preprint. Discussion started: 25 August 2026

WindEurope: Wind energy in Europe: 2023 Statistics and the outlook for 2024–2030, Tech. rep., https://windeurope.org/intelligence-platform/product/wind-energy-in-europe-2023-statistics-and-the-outlook-for-2024-2030/, 2024.